Biallelic Variants in *UBA5* Reveal that Disruption of the UFM1 Cascade Can Result in Early-Onset Encephalopathy

Estelle Colin,[1,2,13] Jens Daniel,[3,13] Alban Ziegler,[1,2,13] Jamal Wakim,[2,13] Aurora Scrivo,[4,13] Tobias B. Haack,[5,13] Salim Khiati,[2] Anne-Sophie Denommé,[1,2] Patrizia Amati-Bonneau,[1,2] Majida Charif,[2] Vincent Procaccio,[1,2] Pascal Reynier,[1,2] Kyrieckos A. Aleck,[6] Lorenzo D. Botto,[7] Claudia Lena Herper,[3] Charlotte Sophia Kaiser,[3] Rima Nabbout,[8] Sylvie N'Guyen,[9] José Antonio Mora-Lorca,[10] Birgit Assmann,[11] Stine Christ,[11] Thomas Meitinger,[5,12] Tim M. Strom,[5,12] Holger Prokisch,[5,12] The FREX Consortium, Antonio Miranda-Vizuete,[10] Georg F. Hoffmann,[11,14] Guy Lenaers,[2,14] Pascale Bomont,[4,14] Eva Liebau,[3,14] and Dominique Bonneau[1,2,14,*]

Via whole-exome sequencing, we identified rare autosomal-recessive variants in *UBA5* in five children from four unrelated families affected with a similar pattern of severe intellectual deficiency, microcephaly, movement disorders, and/or early-onset intractable epilepsy. *UBA5* encodes the E1-activating enzyme of ubiquitin-fold modifier 1 (UFM1), a recently identified ubiquitin-like protein. Biochemical studies of mutant UBA5 proteins and studies in fibroblasts from affected individuals revealed that *UBA5* mutations impair the process of ufmylation, resulting in an abnormal endoplasmic reticulum structure. In *Caenorhabditis elegans*, knockout of *uba-5* and of human orthologous genes in the UFM1 cascade alter cholinergic, but not glutamatergic, neurotransmission. In addition, *uba5* silencing in zebrafish decreased motility while inducing abnormal movements suggestive of seizures. These clinical, biochemical, and experimental findings support our finding of *UBA5* mutations as a pathophysiological cause for early-onset encephalopathies due to abnormal protein ufmylation.

Post-translational modifications (PTM) of proteins by ubiquitin and ubiquitin-like peptides increase the functional diversity of the proteome and are critical regulatory processes involved in many cellular functions including the control of cell cycle, stress response, signaling transduction, and immune response.[1]

The covalent attachment of the ubiquitin-fold modifier 1 (UFM1) to a target protein, also named ufmylation, is a recently identified ubiquitin-like PTM.[2] Similarly to ubiquitination, ufmylation requires a series of enzymes referred to as E1 activating enzyme (UBA5), E2 conjugating enzyme (UFC1), and E3 ligase (UFL1) to transfer UFM1 to its targets.[3] Most members of the UFM1 cascade and target proteins are localized in a large protein complex at the luminal site of the endoplasmic reticulum (ER) and are involved in the regulation of the unfolded protein response (UPR) and ER-stress-mediated apoptosis.[4,5] The UFM1 cascade has also been involved in the development of various cancers[6,7] and other diseases.[5,8,9] However, the specific biological function of ufmylation and the clinical implications of its dysfunction remain largely uncharacterized, even though Duan et al.[10] reported recently the putative involvement of *UBA5* in a single family affected with recessive cerebellar ataxia. Here, we report the involvement of the ufmylation cascade in a severe autosomal-recessive early-onset neurological disorder through the identification of biallelic mutations in *UBA5* (MIM: 610552) in four unrelated families.

This study was approved by the Angers University Hospital Ethics Committee (N° 2016-40). Participants or their parents provided informed, written consent for genetic studies. Using whole-exome sequencing (WES) as a clinical diagnostic tool, we identified rare variants in *UBA5* (GenBank: NM_024818) in two children from a French family (family A, Figure 1). These children developed an early-onset severe neurological disorder consisting of infantile spasms followed by the development of intractable epilepsy, movement disorders, severe intellectual disability, acquired microcephaly, and failure to thrive (Table 1 and Supplemental Note). We excluded a dominant mutation with a germline mosaicism in one of the parents, and X-linked mutations. Then, in the absence of obvious

[1]Department of Biochemistry and Genetics, University Hospital, 49933 Angers Cedex 9, France; [2]UMR CNRS 6214-INSERM 1083 and PREMMI, University of Angers, 49933 Angers Cedex 9, France; [3]Department of Molecular Physiology, Westfälische Wilhelms-University Münster, 48143 Münster, Germany; [4]Avenir-Atip team, INSERM U1051, Institute of Neurosciences of Montpellier, University of Montpellier, 34091 Montpellier Cedex 5, France; [5]Institute of Human Genetics, Technische Universität München, 81675 München, Germany; [6]Department of Genetics and Metabolism, Phoenix Children's Medical Group, Phoenix, AZ 85016, USA; [7]Division of Medical Genetics, Department of Pediatrics, University of Utah, Salt Lake City, UT 84132, USA; [8]Department of Pediatric Neurology, National Reference Center for Rare Epilepsies, University Hospital Necker-Enfants-Malades, 75015 Paris, France; [9]Department of Pediatric Neurology, University Hospital, 49933 Angers Cedex 9, France; [10]Institute of Biomedicine of Seville, University Hospital Virgen del Rocío/CSIC/University of Seville, 41013 Seville, Spain; [11]Department of General Pediatrics, Division of Pediatric Metabolic Medicine and Neuropediatrics, University Hospital Heidelberg, 69120 Heidelberg, Germany; [12]Institute of Human Genetics, Helmholtz Zentrum München, 85764 Neuherberg, Germany
[13]These authors contributed equally to this work
[14]These authors contributed equally to this work
*Correspondence: dobonneau@chu-angers.fr
http://dx.doi.org/10.1016/j.ajhg.2016.06.030.

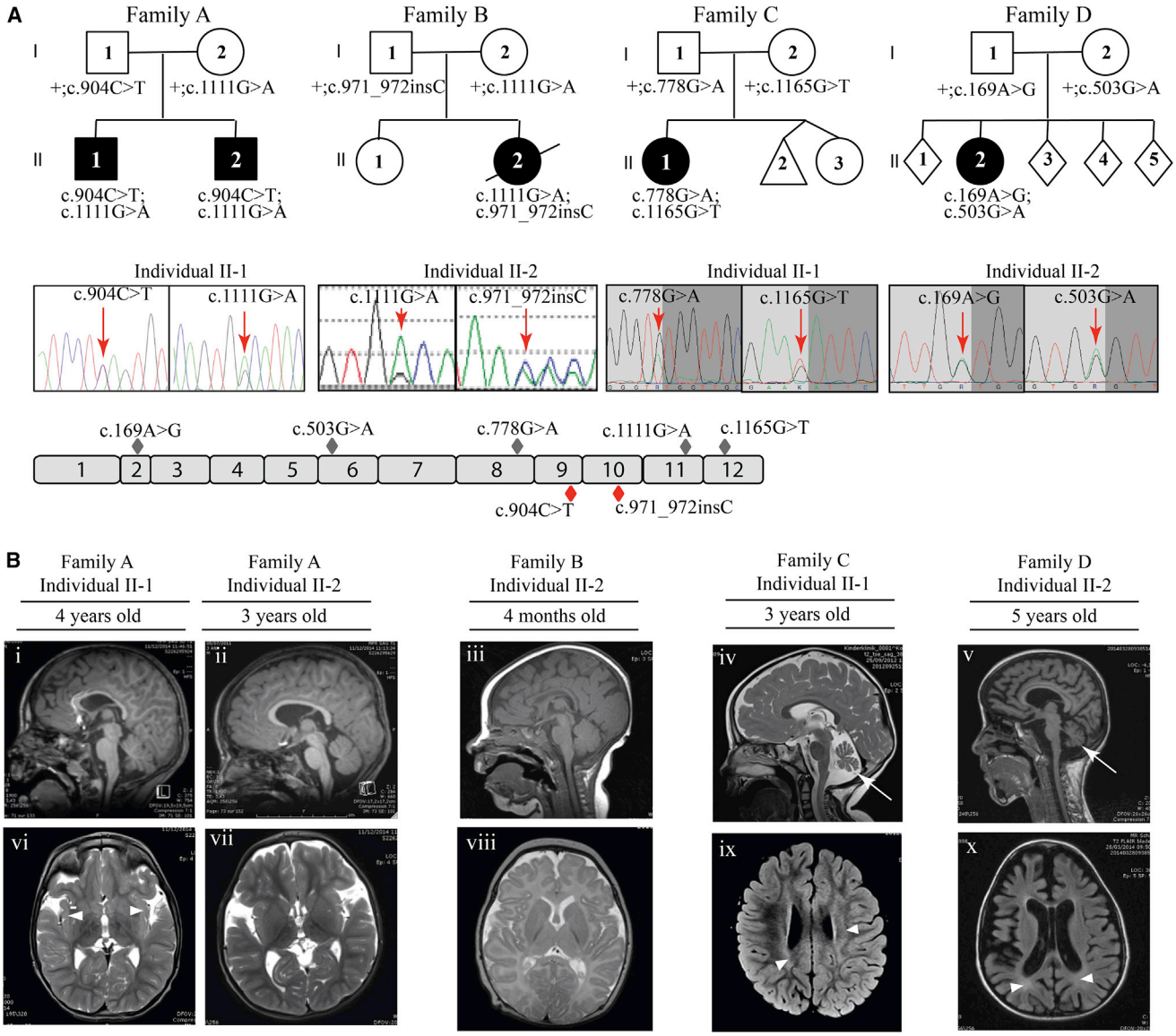

Figure 1. Identification and Segregation of *UBA5* Mutations and Brain MRI of the Five Affected Individuals
(A) Families with mutations in *UBA5*. Filled black symbols represent the affected individuals. Allelic status is given below each tested individual. Representative chromatograms show the compound heterozygous mutations for each family (family A: c.904C>T, c.1111G>A; family B: c.1111G>A, c.971_972insC; family C: c.778G>A, c.1165G>T; family D: c.169A>G, c.503G>A). Red arrows indicate the position of the nucleotide change. Schematic overview of the 12 exons (gray boxes) of human *UBA5*, with missense (gray diamonds) and nonsense (red diamonds) mutations.
(B) Brain MRI of the five affected individuals. Sagittal T1 (i, ii, iii, and v) and sagittal T2 (iv) images are shown. A thin corpus callosum in individuals II-1 from family A, II-2 from family B, and II-2 from family D (i, iii, v), cortical atrophy in individual II-2 from family D (v), and cerebellar atrophy (arrows) without brainstem anomalies in individuals II-1 from family C and II-2 from family D (iv, v) are observed. Axial T2 images (vi, vii, and viii) and T2 Flair (ix, x) are shown. White matter hyperintensities (arrowheads) in insula subcortical white matter (individual II-1 in family A [vi]), periventricular region (individuals II-1 in family C and II-2 in family D [ix, x]), and delayed myelination (individual II-2 in family B) are observed (viii). Widening of sylvian fissures (individuals II-1 and II-2 in family A [vi, vii]) and global cortical atrophy with ventricular dilation (individual II-2 in family D [x]) are observed.

consanguinity and blocks of homozygosity on the SNP array (data not shown), we prioritized WES data filtering for compound-heterozygous damaging variants and found that both children harbored rare biallelic *UBA5* variants (Table 1).

We then evaluated *UBA5* using Sanger sequencing in a cohort of 51 children affected with early-onset epileptic encephalopathy of unknown etiology, and we failed to find any additional case subjects. Next, we contacted several European genetic centers performing WES for genetic determination of unknown disorders and identified two additional unrelated families (C and D, Figure 1A) with rare biallelic variants of *UBA5* (Table 1). In each of these families, the child had severe intellectual disability and movement disorder, but no epilepsy (Table 1 and Supplemental Note).

Table 1. Clinical Features of Individuals with *UBA5* Mutations

Individual	Age (Years)	Sex	Nucleotide and Amino Acid Changes	Hypotonia	Spasticity	Movement Disorder	Epilepsy	ID	Vision Defect	Microcephaly	Brain MRI	EEG Abnormalities	Failure to Thrive
Family A: II-1	5	M	c.1111G>A (p.Ala371Thr); c.904C>T (p.Gln302*)	+	+	+	+	+	+	+	thin corpus callosum, hyperintensities subcortical white matter	+	+
Family A: II-2	4	M	c.1111G>A (p.Ala371Thr); c.904C>T (p.Gln302*)	+	+	–	+	+	+	+	widening of sylvian fissures	+	+
Family B: II-2	2.5	F	c.1111G>A (p.Ala371Thr); c.971_972insC (p.Lys324Asnfs*14)	+	–	–	+	+	+	+	delayed myelination, thin corpus callosum	+	+
Family C: II-1	6	F	c.778G>A (p.Val260Met); c.1165G>T (p.Asp389Tyr)	+	–	+	–	+	+	+	mild cerebellar hypoplasia, white matter hyperintensities	–	+
Family D: II-2	6	F	c.169A>G (p.Met57Val); c.503G>A (p.Gly168Glu)	+	+	+	–	+	+	+	severe cortical atrophy, thin corpus callosum, cerebellar atrophy	–	+

Abbreviations are as follows: M, male; F, female; ID, intellectual deficiency; EEG, electroencephalogram.

An additional child (family B) was identified through the family's blog that mentioned the identification through WES of *UBA5* variants. We contacted this family and the geneticists treating the child and obtained detailed clinical and molecular information (Table 1 and Supplemental Note).

WES was performed on affected children and on their both parents in families A and B and was performed only on affected children in families C and D. WES was performed at Integragen SA (family A), GeneDX (family B), and the Institute of Human Genetics, Helmholtz Center (families C and D). Whole-exome capture was performed using Agilent SureSelect Human All-Exon kit (v.2 for families A, B, and C and v.4 for family D). Sequencing was performed with Illumina Hiseq 2000 or 2500 generating paired-end reads. Average depth of coverage for families A, B, C, and D was 35×, 43×, 134×, and 78×, respectively. More than 91% of targeted regions were covered at least 10 times. DNA sequences were mapped to the reference human genome sequence (UCSC hg19) with Eland V2 for individuals from family A and BWA for individuals from families B, C, and D. CASAVA v.1.8 was used to perform variant calling and annotation for individuals from family A. SAMtools v.0.1.7 was used to detect single-nucleotide variants and small insertions and deletions for individuals from families B, C, and D.

Variants predicted to result in nonsynonymous or frameshift changes were further filtered to prioritize both rare variants with a minor allele frequency (MAF) of less than 1% and novel variants. None of the affected children had rare variant with a MAF of less than 0.1% in any known genes associated with early-onset encephalopathies.

All *UBA5* variants were verified by Sanger sequencing. In all families, the segregation was consistent with a recessive mode of inheritance. We identified a total of seven rare *UBA5* variants including five missense variants, one nonsense variant, and one 1-bp insertion resulting in a frameshift followed by a premature stop codon (Table 1). Notably, all missense variants affected highly conserved amino acid residues (Figure S1). All these variants but one are predicted to be damaging by SIFT, MutationTaster, PolyPhen-2 HVAR, and PROVEAN prediction algorithms (Table S1). The p.Val260Met change is predicted to be neutral and benign by PROVEAN and PolyPhen-2 HVAR but damaging and disease-causing by SIFT and MutationTaster, respectively. Two of the missense variants are recorded in dbSNP 141 and Exome Aggregation Consortium (ExAC) databases: c.1111G>A (p.Ala371Thr) and c.169A>G (p.Met57Val) (Table S1).

In ExAC, the allele frequency of the c.169A>G variant is 8.3×10^{-5}, which is compatible with the expected very low prevalence of the disease. However, the allele frequency of c.1111G>A is 0.0046 in the Finnish population, 0.0028 in the remaining European population, and 0.00297 in the French Exome (FREX) Project database. The calculated prevalence of individuals who are homozygous for this variant would therefore vary from 1/113.370

and 1/128.460 in the French and European populations, respectively, to 1/47,260 in the Finnish population. However, c.1111G>A may act as a hypomorphic allele, as one individual who is homozygous for this allele was identified among 10,490 persons enrolled in the Finnish Sequencing Initiative Suomi (SISu) database. Importantly, this individual, who is in his fifties, is free from any neurological disorder (A.-E. Lehesjoki, personal communication). Nevertheless, in the three individuals with the most severe phenotypes of this study (families A and B), the c.1111G>A allele is associated with a loss-of-function (LOF) allele. Five LOF variants are recorded for *UBA5* in the ExAC database (Table S2) and none in the FREX database. Given the allele frequency of these variants in the European population, the maximum probability that compound heterozygosity of c.1111G>A and a LOF allele would occur by chance is $1/3.06 \times 10^6$ (Table S2), whereas that of c.1111G>A and c.169A>G would be $1/2.62 \times 10^6$. These associations are absent in the ExAC and FREX databases.

Similarly, homozygosity or compound heterozygosyty of LOF alleles would have a maximum frequency of $1/73 \times 10^6$ in the European population. However, the combination of two LOF alleles is likely to be embryonically lethal, as reported for *Uba5* KO mouse[11] and *Drosophila*[10] models. Finally, any other association of pathogenic missense variants cannot be calculated, as they are not recorded in any database.

To analyze the consequences of the seven *UBA5* mutations identified in this study on UFM1 activation, a time-dependent in vitro thioester formation assay was performed as previously described[2] (Figures 2A and S2). We used recombinant UBA5 isoforms reproducing the seven mutations and UFM1 (MIM: 610553), synthesized in fusion with Glutathion-S-Transferase (GST). Reaction mixtures containing one of each UBA5 proteins, UFM1, and ATP were incubated during 0, 2, and 20 min before analyses. Conjugates of UFM1 to UBA5 variants were observed for all UBA5 proteins, except for the p.Gln302* and p.Gly168Glu mutants. Nevertheless, we observed a significantly delayed activity for the p.Met57Val and p.Val260Met proteins and a slightly reduced activity for the p.Ala371Thr and p.Asp389Tyr proteins. Surprisingly, we also found a residual activity for the p.Lys324Asnfs* 14 truncated protein.

We also investigated whether *UBA5* mutations affect UFM1 conjugation to UFC1 using a trans-thioester assay.[2] We incubated UBA5 isoforms with UFM1, UFC1, and ATP for 0, 3, and 30 min (Figures 2B and S3). UBA5-p.Asp389Tyr conjugation activity was similar to WT UBA5, whereas p.Met57Val, p.Val260Met, and p.Ala371Thr proteins had significantly delayed trans-thiol activities and p.Lys324Asnfs*14, p.Gln302*, and p.Gly168Glu proteins had no detectable activity (Figure 2B).

Thus, in vitro UBA5 activation and conjugation assays show that p.Gln302* and p.Gly168Glu proteins are catalytically inactive, whereas p.Met57Val, p.Val260Met, and p.Lys324Asnfs*14 proteins have drastic reductions in catalytic activities. In contrast, the p.Ala371Thr and p.Asp389Tyr protein activities are barely reduced which is consistent with the fact that both amino acid changes are located out of the catalytic domain (aa. 57–329) and which gives an additional argument in favor of hypomorphic alleles.

Notably, the clinical severity of the disorder appears to correlate with residual UBA5 activity. Infantile spasms and pharmacoresistant epilepsy were observed in the three children with a null allele (families A and B) associated with drastically decreased UBA5 activity, whereas children with two missense variants (families C and D) associated with milder impairment of UBA5 activity had developmental delays and movement disorder but no epilepsy.

We also analyzed skin fibroblasts from the two affected children in family A. In a western blot assay, fibroblasts from these individuals, compared to WT fibroblast, showed markedly decreased expression of UBA5 (50% decrease) and ufmylated UBA5 (60% decrease) (Figure 2C). Expression of UFC1, encoding the E2 enzyme of the ufmylation cascade, and UFM1 were increased in the individual's fibroblasts compared to WT fibroblasts (Figure 2D and 2E). UBA5 ufmylation after a 24 hr-long tunicamycin (TM) treatment was increased in WT cells, while mutant cells were unable to increase UBA5 ufmylation (Figure 2F). In addition, mutant cells were resistant to TM long exposure and showed similar pro-apoptotic staurosporine sensitivity as WT cells (Figure S4). Confocal live cell imaging revealed an expanded ER network in *UBA5* mutant compared to WT fibroblasts (Figure 2G). Taken together, these results indicate that the ufmylation pathway is defective in *UBA5* mutant fibroblasts, with decreased content of UBA5 and increased content of UFC1 and UFM1.

At a cellular level in mutant fibroblasts, the ER volume is increased and response to TM treatment is deficient. Both of these features are typically observed in cells suffering from ER stress.

The Ufm1 cascade in *C. elegans* is evolutionarily conserved, with similar targets as in humans.[12] Thus, we analyzed the neurotransmission capacity of worm carrying deletions in the genes encoding for the E1 enzyme Uba5, the protease Ufsp2, and for the ufmylation targets Ufbp1 or Cdkr3, using aldicarb, an Ach esterase inhibitor, and pentylenetetrazole (PTZ), a GABA receptor antagonist.[13]

Wild-type (N2 Bristol)[14] and Ufm1 cascade mutant worms (Table S3) did not show a seizure phenotype in the presence of PTZ, whereas PTZ-sensitive worms (*unc-43*)[15] showed severe seizure phenotypes (data not shown). However, compared to WT animals, all Ufm1 cascade mutants displayed a significantly higher rate of pharynx grinder paralysis in the presence of aldicarb (Figure 3A), pointing to a pathophysiological mechanism involving an increased amount of ACh in the neuromuscular junctions.[13] Our data are consistent with those obtained in a *Drosophila* model in which UBA5 knockdown induced

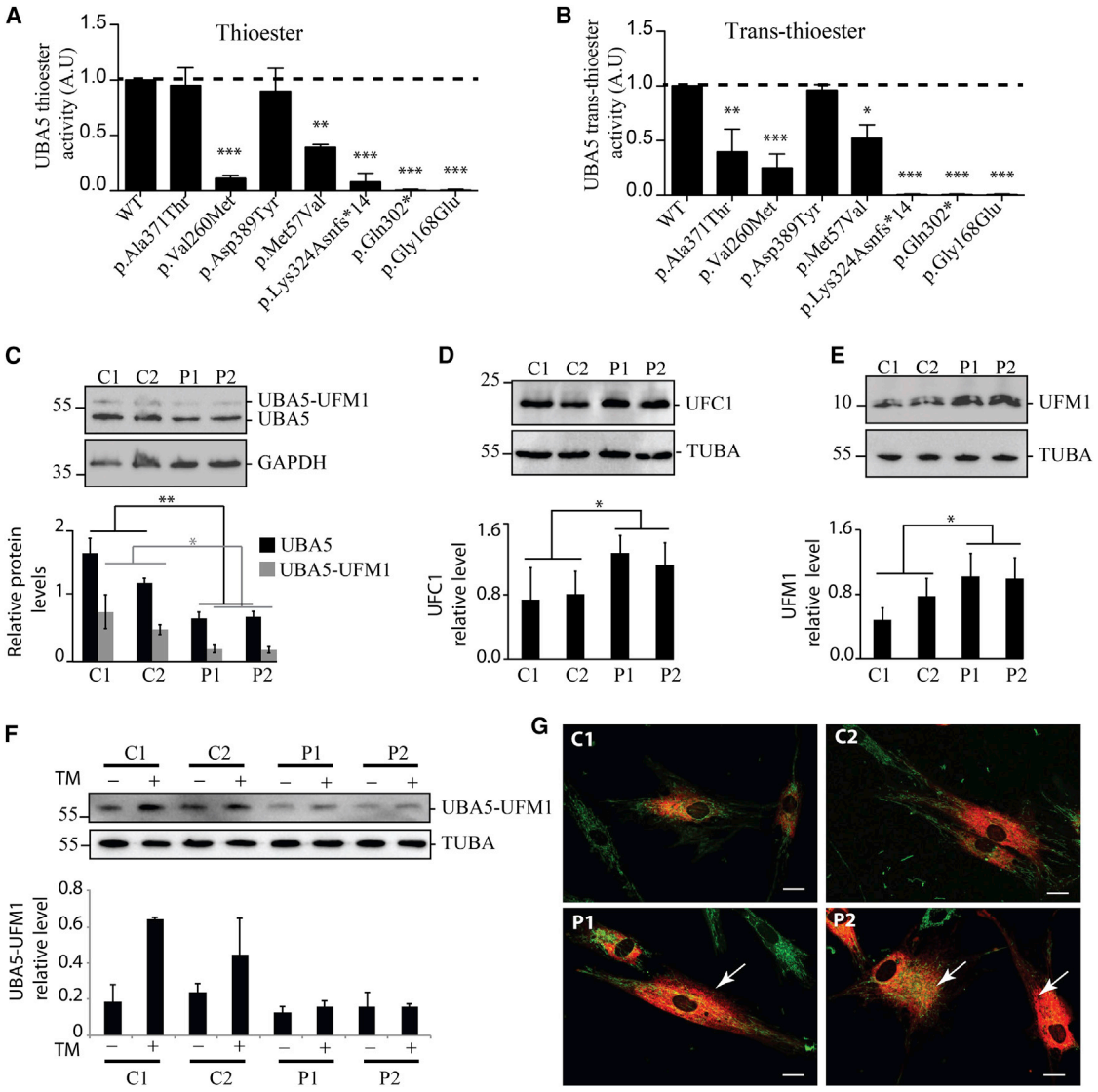

Figure 2. Biochemical and Cellular Characterization of the UBA5 Disease-Causing Variants

(A and B) UBA5, UFM1, and UFC1 recombinant proteins were produced in *E. coli*, purified, and used for in vitro UFM1 thioester activation and trans-thioester conjugation reactions, according to published protocols.[2]

(A) In vitro assessment of UFM1 thioester activation by the UBA5-Glutathion-S-Transferase (GST) fusion proteins, each carrying one of the mutations of the affected families. The thioester formations were monitored after 2 min of incubation.

(B) Assessment of UFM1 trans-thioester conjugation to UFC1 by the UBA5-GST fusion proteins carrying each one of the mutations of the affected families. The trans-thioester formations were monitored after 3 min of incubation.

Three independent experiments were used for quantification and statistical analyses by one-way ANOVA, Bonferroni's multiple comparison test, *$p < 0.05$, **$p < 0.01$, ***$p < 0.001$.

(C–G) Skin fibroblasts from the two affected individuals from family A (P1 equate to II-1 and P2 equate to II-2) and from two control subjects were grown in DMEM-F12 for 24 hr and used for assessing the UFM1 cascade.

(C) Representative western blots (top) of free (lower bands) and ufmylated (upper bands) UBA5 (Proteintech cat# 12093-1-AP, RRID: AB_2211743) and GAPDH (GeneTex cat# GTX100118, RRID: AB_1080976) proteins in control (C1, C2) and *UBA5* mutant (P1, P2) fibroblast protein extracts, and quantification (bottom) of the relative levels of UBA5/GAPDH and UBA5-UFM1/GAPDH.

(D) Representative western blots (top) of UFC1 (Abcam cat# ab189251) and quantification (bottom) of UFC1 expression level related to TUBA (Sigma-Aldrich cat# T9026, RRID: AB_477593).

(E) Representative western blots (top) in non-reducing conditions (using Optiblot LDS Sample buffer, Abcam) of free UFM1 (Abcam cat# ab109305, RRID: AB_10864) and quantification (bottom) of UFM1 expression level related to TUBA.

(F) Representative western blots (top) of UBA5 ufmylation with (+) and without (−) 10 μg/mL of tunicamycin (TM, BML-CC104, Enzo Life Sciences) treatment for 24 hr and quantification (bottom) related to TUBA. Three independent experiments were used for quantification and statistical analyses using Student's t test, *$p < 0.05$; **$p < 0.01$.

(G) Confocal live images of WT (C1, C2) and UBA5 mutant (P1, P2) fibroblasts transduced by an RFP-tagged ER red probe (C10591, CellLight ER-RFP, BacMam 2.0, Thermo Fischer Scientific), and stained with MitoTracker-green (M7514, Thermofisher) to reveal the ER and mitochondria. Arrows highlight expanded ER network in *UBA5* mutant fibroblasts. Scale bar represents 10 μm.

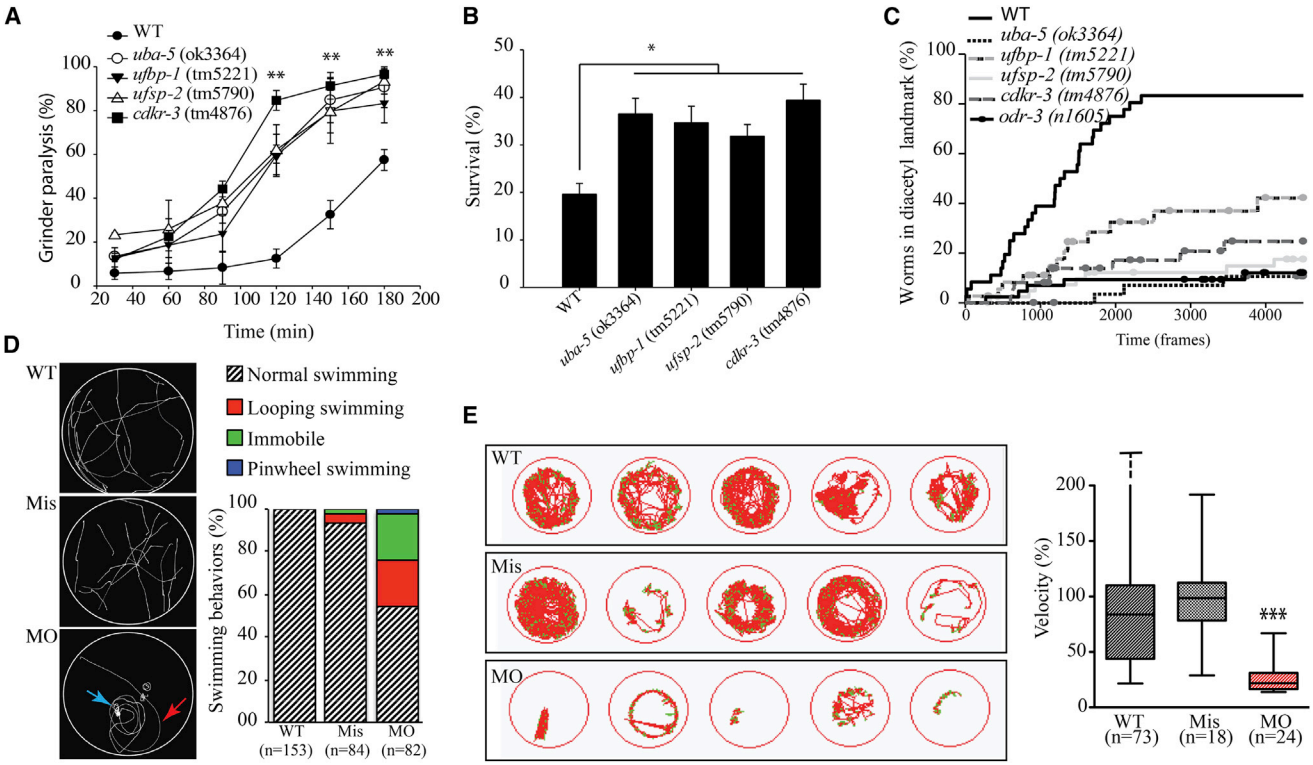

Figure 3. Characterization of *C. elegans* Strains Deleted for Genes Involved in Ufmylation and Zebrafish Silenced for *uba5*

(A–C) *C. elegans* UFM-1 cascade deletion strains *uba-5(ok3364)*, *ufbp-1(tm5221)*, *ufsp-2(tm5790)*, and *cdkr-3(tm4876)* were used for the following experiments and compared to the wild-type (WT) strain (N2 Bristol).

(A) Assessment of grinder paralysis of the UFM-1 cascade deletion strains treated with 0.5 mM aldicarb for 60 min reveal that the mutants display a highly significant increase in grinder paralysis, witnessing failure to negatively regulate acetylcholine release (ANOVA, $^{**}p < 0.01$).

(B) Assessment of survival of the UFM-1 cascade deletion strains, after an 18 hr treatment with the ER-stressor dithiothreitol (DTT, 11 mM), show that mutants are resistant to ER stress, compared to WT animals (ANOVA, $^{*}p < 0.05$).

(C) Assessment of chemotaxis toward the attractant diacetyl of the UFM-1 cascade deletion strains shows that the percentage of animals entering the landmark containing diacetyl (1/1,000) was significantly lower for the UFM-1 cascade deletion mutants compared to WT (Kaplan-Meier curve, $p < 0.01$). Negative control *odr-3(n1605)* worms were unable to sense diacetyl. Trajectories of the worms were recorded for 7.5 min with 10 frames per second via the FTIR-based Imaging Method (FIM).[26]

(D and E) Zebrafish from the AB genetic background were maintained at 28°C on a 14 hr light and 10 hr dark cycle, and fertilized eggs were injected with the antisense *uba5* morpholino oligonucleotide (MO) and the mismatch oligonucleotide (Mis) at a concentration of 0.35 pM.

(D) Assessment of 72 hpf larvae motility, after a slight mechanical stimulation on the tail. The motion of individual larvae was examined (left) and scored (right) as normal swimming, looping swimming (red arrow), pinwheel swimming (blue arrow), or immobile and revealed a significant and specific alteration of swimming in uba5-depleted animals (MO), compared to larvae injected with the mismatch morpholino (Mis) and control larvae (WT). Quantification of the swimming behavior showed a normal motility for WT and Mis-injected larvae, whereas 45.1% of the MO showed impaired motility: 22% were immobile, 20.7% exhibited looping swimming, and 2.4% showed pinwheel swimming.

(E) Spontaneous motility of zebrafish monitored at 5 days post fertilization (dpf) using the Zebrabox recording system (Viewpoint). The cumulative movement of representative WT, Mis, and MO larvae is represented (left). The quantification of the velocity (right, mm/s), expressed as percentages of the WT values, revealed a significant decreased motility in uba5-depleted zebrafish ($^{***}p < 0.001$ between WT/MO and between Mis/MO but not significant between WT/Mis; statistical significance was inferred with the non-parametric Mann-Whitney test). Horizontal bars in the boxes represent the median values, horizontal bars outside the boxes represent the maximal and minimal individual values (in the WT, the maximal individual value was 676%).

locomotive defects, a shortened lifespan, and aberrant neuromuscular junctions (NMJs).[10] Treatment with levamisole, an ACh receptor agonist known to paralyze worms,[16] did not induce differences in motility between control and mutant worms (Figure S5), suggesting that the alteration of Ufm1 cascade and of Ufbp1 and Cdkr3 induce increased ACh release in neuromuscular junctions. Although it is premature to directly extrapolate these results to brain dysfunction in humans, it is interesting to note the established associations between ACh neuron function and severe central neurological disorders. First, mutations in *CHRNA4* (MIM: 118504), *CHRNB2* (MIM: 118507), and *CHRNA2* (MIM: 118502), encoding nicotinic acetylcholine receptor (nAChR) α and β subunits, cause autosomal-dominant nocturnal frontal lobe epilepsy (ADNFLE [MIM: 600513]), an epileptic disorder with clusters of motor seizures occurring predominantly during sleep.[17,18] In addition, neuronal nAChRs participating in synaptic plasticity

are involved in learning, memory, and brain development.[19] Second, disruptions or alterations of nicotinic cholinergic mechanisms are involved in neurological disorders, including epilepsy, schizophrenia, Parkinson disease, dementia with Lewy bodies, and Alzheimer disease.[19] Finally, a selective reduction in acetylcholinergic neurons (AChNs) has been found in the pedunculopontine tegmental nucleus of people with refractory epilepsy including infantile spasms.[20] Although these findings support a role for AChNs dysfunction in neurologic disorders (including some with epilepsy), it is fair to conclude that the specific chain of events from UBA5 dysfunction to the associated clinical condition reported here (with refractory epilepsy, movement disorders, and severe developmental delay) remains largely uncharacterized—an unsurprising situation given the complexity of the cholinergic regulation in both developing and mature brains.[21]

In addition, because *C. elegans uba-5(ok3364)* mutants are resistant to ER stress,[12] we monitored the effect of dithiothreitol (DDT) treatment on all Ufm1 cascade mutants and found that, compared to WT, they were resistant to ER stress (Figure 3B). Therefore, both in mutated fibroblasts and in *C. elegans*, alteration of the Ufm1 cascade induces ER-stress resistance, although without triggering the unfolded protein response (UPR; data not shown). Together, these data suggest that a close connection exists between ufmylation and ER physiology, without pointing to the UPR as the culprit mechanism in this disease. Our results further suggest that the ufmylation targets UFBP1 and CDK5RAP3, which are involved in functions downstream of UFM1 cascade,[5,6,22–24] might play a crucial role in the pathogenicity of the disease. Indeed, these proteins aggregate in a large complex with UFL1 and UFSP2 at the ER membrane,[5,6,23,25] and CDK5RAP3 decreases the kinase activity of CDK5, which mutations are responsible for a severe form of epileptic encephalopathy associated with lissencephaly.[26]

In a next step, using a computer-aided chemotaxis assay, we analyzed the effects of the Ufm1 cascade on *C. elegans* sensorial behavior by a chemotaxis assay with the attractant diacetyl.[27] Results revealed a decreased ability in sensing diacetyl in all mutants compared to WT animals (Figure 3C), pointing to a failure in the *C. elegans* sensory system in the absence of the Ufm1 cascade and its targets.

Finally, we examined the phenotype of zebrafish (*Danio rerio*) silenced for *uba5*. We first identified the single *uba5* ortholog gene in the zebrafish genome (GenBank: NP_001292546.1), which encodes a protein sharing 80% identity with human UBA5. The *uba5* morpholinos (MOs) and mismatch MOs (Mis) (Gene Tools) were designed against the splice junction between intron 1 and exon 2 of the zebrafish *uba5*. Embryos injected with *uba5*-MO or control *uba5*-Mis did not reveal morphological alteration in comparison to non-injected WT embryos at 24, 48, and 72 hr post fertilization (hpf) (data not shown), indicating a normal development of uba5-depleted larvae. Nevertheless, the motility of the morphants was considerably altered, as suspected by their decreased movements and difficulty to exit the chorion (data not show). To quantify the motility defect, we examined the touch-escape response of larvae at 72 hpf. Although WT and *uba5*-Mis injected larvae exhibited linear movement upon stimulation, morphants were either unable to move or exhibited looping or pinwheel swimming (Figure 3D, showing representative traces of Movies S1, S2, and S3). The analysis of large populations revealed a pronounced impaired motility in 45.1% of the *uba5*-MO-injected larvae (Figure 3D, Movies S4, S5, and S6), with predominant looping (37% of the mobile morphants). To further characterize the motor activity of uba5-depeleted zebrafishes, we tracked the spontaneous motility of 5-day-old larvae, which revealed a severe and specific decrease in morphant motility (Figure 3E). Thus, silencing of *uba5* in zebrafish resulted in seizure-like behavior[28,29] and decreased locomotor function, both reminiscent of clinical phenotypes in the most severely affected children in this study. The findings underscore the crucial importance of UBA5 activity and thereby protein ufmylation in central nervous system function.

Further suggestive evidence linking ufmylation to neurological disorders derives from the observation that UFC1 and UFM1 colocalize with NCAM on the cell surface of neurons.[30] NCAM is a neural cell adhesion molecule implicated in axon growth, neuronal differentiation, and synaptic plasticity in brain. UFM1 overexpression also increases the endocytosis of NCAM, a process that has to be fine-tuned for proper nervous system development.[31] Finally, interactors of the ufmylation cascade have been found using mass spectrometry,[32] including USP9X, which is required for proper neural cell migration and axonal growth. Loss-of-function mutations of *USP9X* (MIM: 300072) cause an X-linked intellectual disability.[33]

In summary, we report clinical, molecular, and experimental evidence indicating that biallelic *UBA5* mutations cause early-onset encephalopathy characterized by seizures, developmental delays, and movement disorders. We suggest that adding *UBA5* to gene panels targeted to individuals with early-onset refractory seizures or movement disorders accompanied by severe intellectual deficiency could increase the diagnostic yield and help with clinical management and genetic counseling.

Accession Numbers

Whole-exome sequencing data for family A have been deposited in the European Nucleotide Archive (ENA) with accession PRJEB9854. The GenBank accession number for zebrafish mmp21 is KT207790.

Supplemental Data

Supplemental Data include a clinical note, five figures, three tables, and six movies and can be found with this article online at http://dx.doi.org/10.1016/j.ajhg.2016.06.030.

Consortia

The FREX Consortium's principal investigators are Emmanuelle Génin, Dominique Campion, Jean-François Dartigues, Jean-François Deleuze, Jean-Charles Lambert, and Richard Redon. Collaborators are as follows: bioinformatics group (Thomas Ludwig, Benjamin Grenier-Boley, Sébastien Letort, Pierre Lindenbaum, Vincent Meyer, Olivier Quenez), statistical genetics group (Christian Dina, Céline Bellenguez, Camille Charbonnier-Le Clézio, Joanna Giemza), data collection (Stéphanie Chatel, Claude Férec, Hervé Le Marec, Luc Letenneur, Gaël Nicolas, Karen Rouault), and sequencing (Delphine Bacq, Anne Boland, Doris Lechner).

Acknowledgments

We thank all the families for their participation in this study. We thank INSERM and CNRS, the Region Pays de la Loire, Angers Loire-Métropole, University of Angers, and University Hospital of Angers for their financial support to the PREMMI project, the University of Montpellier for institutional support, the German Bundesministerium für Bildung und Forschung through the German Network for mitochondrial disorders (mitoNET, 01GM1113C to T.M. and H.P.), and the E-Rare project GENOMIT (01GM1207 for T.M. and H.P.). T.B.H. was supported by the BMBF through the Juniorverbund in der Systemmedizin "mitOmics" (FKZ 01ZX1405C). This work was also supported by France Génomique National infrastructure, funded as part of "Investissement d'avenir" program managed by Agence Nationale pour la Recherche. We thank the Caenorhabditis Genetics Center and the National Bioresource Project for the Experimental Animal Nematode *C. elegans* (NBRP) for providing us with knockout strains. We thank C. Klämbt, B. Risse, N. Otto, and D. Berh for the opportunity to use the FIMtrack system for chemotaxis assay on *C. elegans* and for their support in data analysis. We thank Mr. Cubedo and Dr. Rossel for hosting zebrafish (INSERM U710) and C. Conan for performing the touch-response test. A.S. is funded by the Région Languedoc-Roussillon and P.B. is supported by grants from the Avenir-Atip program from INSERM and the CNRS, the Région Languedoc-Roussillon, and the Association Française contre les Myopathies. We thank Delphine Heron for having tested UBA5 in children affected with early encephalopathy and Joanne Walker and Kanaya Malkani for critical reading of the manuscript.

Received: January 27, 2016
Accepted: June 28, 2016
Published: August 18, 2016

Web Resources

BLAST, http://blast.ncbi.nlm.nih.gov/Blast.cgi
dbSNP, http://www.ncbi.nlm.nih.gov/projects/SNP/
Ensembl Genome Browser, http://www.ensembl.org/index.html
European Nucleotide Archive, http://www.ebi.ac.uk/ena
ExAC Browser, http://exac.broadinstitute.org/
France Génomique (FREX) Project, https://www.france-genomique.org/spip/
GenBank, http://www.ncbi.nlm.nih.gov/genbank/
GeneCards, http://www.genecards.org
Morpholinos (Gene Tools), http://www.gene-tools.com/morpholino_antisense_oligos
MutationTaster, http://www.mutationtaster.org/
OMIM, http://www.omim.org/
PolyPhen-2, http://genetics.bwh.harvard.edu/pph2/
Primer3, http://bioinfo.ut.ee/primer3
PROVEAN, http://provean.jcvi.org
RefSeq, http://www.ncbi.nlm.nih.gov/RefSeq
RRID, https://scicrunch.org/resources
SIFT, http://sift.bii.a-star.edu.sg/
SISu Project, http://www.sisuproject.fi/
The Human Protein Atlas, http://www.proteinatlas.org/
ZFIN: BLAST Query, https://zfin.org/action/blast/blast

References

1. van der Veen, A.G., and Ploegh, H.L. (2012). Ubiquitin-like proteins. Annu. Rev. Biochem. *81*, 323–357.
2. Komatsu, M., Chiba, T., Tatsumi, K., Iemura, S., Tanida, I., Okazaki, N., Ueno, T., Kominami, E., Natsume, T., and Tanaka, K. (2004). A novel protein-conjugating system for Ufm1, a ubiquitin-fold modifier. EMBO J. *23*, 1977–1986.
3. Daniel, J., and Liebau, E. (2014). The ufm1 cascade. Cells *3*, 627–638.
4. Zhang, M., Zhu, X., Zhang, Y., Cai, Y., Chen, J., Sivaprakasam, S., Gurav, A., Pi, W., Makala, L., Wu, J., et al. (2015). RCAD/Ufl1, a Ufm1 E3 ligase, is essential for hematopoietic stem cell function and murine hematopoiesis. Cell Death Differ. *22*, 1922–1934.
5. Lemaire, K., Moura, R.F., Granvik, M., Igoillo-Esteve, M., Hohmeier, H.E., Hendrickx, N., Newgard, C.B., Waelkens, E., Cnop, M., and Schuit, F. (2011). Ubiquitin fold modifier 1 (UFM1) and its target UFBP1 protect pancreatic beta cells from ER stress-induced apoptosis. PLoS ONE *6*, e18517.
6. Wu, J., Lei, G., Mei, M., Tang, Y., and Li, H. (2010). A novel C53/LZAP-interacting protein regulates stability of C53/LZAP and DDRGK domain-containing Protein 1 (DDRGK1) and modulates NF-kappaB signaling. J. Biol. Chem. *285*, 15126–15136.
7. Yoo, H.M., Park, J.H., Jeon, Y.J., and Chung, C.H. (2015). Ubiquitin-fold modifier 1 acts as a positive regulator of breast cancer. Front. Endocrinol. (Lausanne) *6*, 36.
8. Liu, H., Li, J., Tillman, B., French, B.A., and French, S.W. (2014). Ufmylation and FATylation pathways are downregulated in human alcoholic and nonalcoholic steatohepatitis, and mice fed DDC, where Mallory-Denk bodies (MDBs) form. Exp. Mol. Pathol. *97*, 81–88.
9. Azfer, A., Niu, J., Rogers, L.M., Adamski, F.M., and Kolattukudy, P.E. (2006). Activation of endoplasmic reticulum stress response during the development of ischemic heart disease. Am. J. Physiol. Heart Circ. Physiol. *291*, H1411–H1420.
10. Duan, R., Shi, Y., Yu, L., Zhang, G., Li, J., Lin, Y., Guo, J., Wang, J., Shen, L., Jiang, H., et al. (2016). UBA5 mutations cause a new form of autosomal recessive cerebellar ataxia. PLoS ONE *11*, e0149039.
11. Tatsumi, K., Yamamoto-Mukai, H., Shimizu, R., Waguri, S., Sou, Y.-S., Sakamoto, A., Taya, C., Shitara, H., Hara, T., Chung, C.H., et al. (2011). The Ufm1-activating enzyme Uba5 is indispensable for erythroid differentiation in mice. Nat. Commun. *2*, 181.
12. Hertel, P., Daniel, J., Stegehake, D., Vaupel, H., Kailayangiri, S., Gruel, C., Woltersdorf, C., and Liebau, E. (2013). The

ubiquitin-fold modifier 1 (Ufm1) cascade of *Caenorhabditis elegans*. J. Biol. Chem. *288*, 10661–10671.
13. Locke, C., Berry, K., Kautu, B., Lee, K., Caldwell, K., and Caldwell, G. (2008). Paradigms for pharmacological characterization of *C. elegans* synaptic transmission mutants. J. Vis. Exp. *18*, e837.
14. Brenner, S. (1974). The genetics of *Caenorhabditis elegans*. Genetics *77*, 71–94.
15. Vashlishan, A.B., Madison, J.M., Dybbs, M., Bai, J., Sieburth, D., Ch'ng, Q., Tavazoie, M., and Kaplan, J.M. (2008). An RNAi screen identifies genes that regulate GABA synapses. Neuron *58*, 346–361.
16. Martin, R.J., Robertson, A.P., Buxton, S.K., Beech, R.N., Charvet, C.L., and Neveu, C. (2012). Levamisole receptors: a second awakening. Trends Parasitol. *28*, 289–296.
17. Steinlein, O.K., Mulley, J.C., Propping, P., Wallace, R.H., Phillips, H.A., Sutherland, G.R., Scheffer, I.E., and Berkovic, S.F. (1995). A missense mutation in the neuronal nicotinic acetylcholine receptor alpha 4 subunit is associated with autosomal dominant nocturnal frontal lobe epilepsy. Nat. Genet. *11*, 201–203.
18. Aridon, P., Marini, C., Di Resta, C., Brilli, E., De Fusco, M., Politi, F., Parrini, E., Manfredi, I., Pisano, T., Pruna, D., et al. (2006). Increased sensitivity of the neuronal nicotinic receptor alpha 2 subunit causes familial epilepsy with nocturnal wandering and ictal fear. Am. J. Hum. Genet. *79*, 342–350.
19. Dani, J.A., and Bertrand, D. (2007). Nicotinic acetylcholine receptors and nicotinic cholinergic mechanisms of the central nervous system. Annu. Rev. Pharmacol. Toxicol. *47*, 699–729.
20. Hayashi, M., Nakajima, K., Miyata, R., Tanuma, N., and Kodama, T. (2012). Lesions of acetylcholine neurons in refractory epilepsy. ISRN Neurol. *2012*, 404263.
21. Becchetti, A., Aracri, P., Meneghini, S., Brusco, S., and Amadeo, A. (2015). The role of nicotinic acetylcholine receptors in autosomal dominant nocturnal frontal lobe epilepsy. Front. Physiol. *6*, 22.
22. Kim, C.H., Nam, H.-S., Lee, E.H., Han, S.H., Cho, H.J., Chung, H.J., Lee, N.S., Choi, S.J., Kim, H., Ryu, J.S., et al. (2013). Overexpression of a novel regulator of p120 catenin, NLBP, promotes lung adenocarcinoma proliferation. Cell Cycle *12*, 2443–2453.
23. Shiwaku, H., Yoshimura, N., Tamura, T., Sone, M., Ogishima, S., Watase, K., Tagawa, K., and Okazawa, H. (2010). Suppression of the novel ER protein Maxer by mutant ataxin-1 in Bergman glia contributes to non-cell-autonomous toxicity. EMBO J. *29*, 2446–2460.
24. Cai, Y., Pi, W., Sivaprakasam, S., Zhu, X., Zhang, M., Chen, J., Makala, L., Lu, C., Wu, J., Teng, Y., et al. (2015). UFBP1, a key component of the Ufm1 conjugation system, is essential for ufmylation-mediated regulation of erythroid development. PLoS Genet. *11*, e1005643.
25. Kwon, J., Cho, H.J., Han, S.H., No, J.G., Kwon, J.Y., and Kim, H. (2010). A novel LZAP-binding protein, NLBP, inhibits cell invasion. J. Biol. Chem. *285*, 12232–12240.
26. Magen, D., Ofir, A., Berger, L., Goldsher, D., Eran, A., Katib, N., Nijem, Y., Vlodavsky, E., Tzur, S., Behar, D.M., et al. (2015). Autosomal recessive lissencephaly with cerebellar hypoplasia is associated with a loss-of-function mutation in CDK5. Hum. Genet. *134*, 305–314.
27. Risse, B., Thomas, S., Otto, N., Löpmeier, T., Valkov, D., Jiang, X., and Klämbt, C. (2013). FIM, a novel FTIR-based imaging method for high throughput locomotion analysis. PLoS ONE *8*, e53963.
28. Baraban, S.C., Taylor, M.R., Castro, P.A., and Baier, H. (2005). Pentylenetetrazole induced changes in zebrafish behavior, neural activity and c-fos expression. Neuroscience *131*, 759–768.
29. Stewart, A.M., Desmond, D., Kyzar, E., Gaikwad, S., Roth, A., Riehl, R., Collins, C., Monnig, L., Green, J., and Kalueff, A.V. (2012). Perspectives of zebrafish models of epilepsy: what, how and where next? Brain Res. Bull. *87*, 135–143.
30. Homrich, M., Wobst, H., Laurini, C., Sabrowski, J., Schmitz, B., and Diestel, S. (2014). Cytoplasmic domain of NCAM140 interacts with ubiquitin-fold modifier-conjugating enzyme-1 (Ufc1). Exp. Cell Res. *324*, 192–199.
31. Rutishauser, U. (2008). Polysialic acid in the plasticity of the developing and adult vertebrate nervous system. Nat. Rev. Neurosci. *9*, 26–35.
32. Havugimana, P.C., Hart, G.T., Nepusz, T., Yang, H., Turinsky, A.L., Li, Z., Wang, P.I., Boutz, D.R., Fong, V., Phanse, S., et al. (2012). A census of human soluble protein complexes. Cell *150*, 1068–1081.
33. Homan, C.C., Kumar, R., Nguyen, L.S., Haan, E., Raymond, F.L., Abidi, F., Raynaud, M., Schwartz, C.E., Wood, S.A., Gecz, J., and Jolly, L.A. (2014). Mutations in USP9X are associated with X-linked intellectual disability and disrupt neuronal cell migration and growth. Am. J. Hum. Genet. *94*, 470–478.

The American Journal of Human Genetics, Volume *99*

Supplemental Data

Biallelic Variants in *UBA5* Reveal that Disruption of the UFM1 Cascade Can Result in Early-Onset Encephalopathy

Estelle Colin, Jens Daniel, Alban Ziegler, Jamal Wakim, Aurora Scrivo, Tobias B. Haack, Salim Khiati, Anne-Sophie Denommé, Patrizia Amati-Bonneau, Majida Charif, Vincent Procaccio, Pascal Reynier, Kyrieckos A. Aleck, Lorenzo D. Botto, Claudia Lena Herper, Charlotte Sophia Kaiser, Rima Nabbout, Sylvie N'Guyen, José Antonio Mora-Lorca, Birgit Assmann, Stine Christ, Thomas Meitinger, Tim M. Strom, Holger Prokisch, The FREX Consortium, Antonio Miranda-Vizuete, Georg F. Hoffmann, Guy Lenaers, Pascale Bomont, Eva Liebau, and Dominique Bonneau

Supplemental Note 1: Case reports

Case 1 (Family A, Individual II-1)

Individual 1 is a boy born to healthy non-consanguineous French parents. After a normal pregnancy, delivery was vaginal at 40 weeks of gestation. Growth characteristics at birth were normal: weight 3.48 kg, length 51cm, and occipitofrontal circumference (OFC) 36cm. Until 3 months of age, the child's development was considered normal. At age 3 months, he presented infantile spasms with a hypsarrhythmic EEG pattern, i.e. the West syndrome, associated with signs of failure to thrive. Seizures were refractory to polytherapy including vigabatrin, sodium valproate, clobazam, and corticosteroid. A ketogenic diet, started at age 20 months, initially decreased the frequency of seizures with an improved EEG pattern, but within a few months the seizures worsened, requiring further changes in treatment. On examination, at age 5 years, he had familial (non-dysmorphic) facial features, and still manifested significant failure to thrive despite gastric tube feeding. His length was then 91 cm (-4 SD), weight 10 kg (-4SD) and OFC 47cm (-3.5sd). He was minimally responsive to his environment, had no head control, no language skills, and could not sit up unaided. Axial hypotonia was associated with peripheral hypertonia. Visual pursuit was inconstantly present. Generalized tonic-clonic seizures occurred several times a day despite anticonvulsant polytherapy. Normal testing included plasma and cerebrospinal fluid (CSF) lactate, plasma and CSF amino acids, CSF glucose, neurotransmitters and interferon, urine organic acids, plasma and urine creatine and guanidinoacetate, plasma purines and pyrimidines, biotinidase, very long chain fatty acids, plasma phytanic and prystanic acid, plasma copper and ceruloplasmin. Screening for congenital disorders of glycosylation was done *via* plasmatic glycoprotein analyses. Sanger sequencing of *MECP2, STXBP1, CDKL5, FOXG1* and *ARX* showed no mutation. Brain CT-scan and MRI at the age of 3 months were normal. However,

subsequent brain MRIs at 15 months and 4.5 years showed a thin corpus callosum and hyperintensities in insula subcortical white matter (Figure 1B, a,f).

Case 2 (Family A, Individual II-2)

Individual 2 is brother to Individual 1. Pregnancy and delivery (vaginal, at 40 weeks of gestation) were uneventful. The growth characteristics at birth were normal: weight 3.3 kg, length 50cm, and OFC 35cm. Head control was acquired at age 2 months, but at age 4 months he had infantile spasms and showed signs of failure to thrive. Treatment with clobazam and corticotherapy, together with a ketogenic diet at age 5 months, initially resulted in a moderate reduction of seizures. Blinking reflexes and pupillary light reflexes were decreased but fundus examination and electroretinograms were normal. Corticotherapy was tapered down and stopped at age 7 months. Because of subsequent worsening of the EEG pattern at age 15 months, clobazam was discontinued and clonazepam was added. At age 27 months, he was presenting daily seizures with a prolonged postictal state. The ketogenic diet was stopped and sodium valproate was introduced. However, there was no improvement in seizure control. At age 4 years, he showed familial (non-dysmorphic) features, with severe developmental delay, with no head control, inability to sit up unaided, and no language skills. He presented axial hypotonia with peripheral hypertonia. Despite anticonvulsant polytherapy, generalized myoclonic seizures occurred several times a day. Visual pursuit was inconstantly present. Like his brother, he showed signs of failure to thrive, with length 89 cm (-2SD), weight 9.6kg (-3.5SD) and OFC 47cm (-2SD), leading to the insertion of a gastrostomy feeding tube. Extensive metabolic screening in blood, urine, and CSF was negative. Brain MRI at age 4 months was normal. However, a subsequent MRI at age 3 years showed widening of sylvian fissures (Figure 1B, b,g).

Case 3 (Family B, Individual II-2)

Individual 3 was a girl, the second child of healthy non-consanguineous American parents without a family history. Delivery was vaginal at 35 weeks of gestation after a pregnancy complicated by hyperemesis gravidarum. At birth, her weight was 2.8 kg and the OFC was 33 cm (4th centile); the perinatal evaluation was normal. The seizures, associated with feeding difficulties, began at the age of 2 months. She developed infantile spasms with hypsarrhythmia at the age of 5 months. These spasms proved refractory to drugs. A gastrostomy was placed at the age of 1 year. She acquired the ability to smile at age 13 months, but then lost it. Iterative brain MRI evidenced delayed myelination (Figure 1B, c,h). Normal results were found with assays of urine amino and organic acids, plasma amino acids, urine oligosaccharide and mucopolysaccharides, lysosomal enzymes, plasma VLCFA, and CDG screening. SNP-array and Sanger sequencing of *FOXG1* and of the genes responsible for neuronal ceroid lipofuscinose (*PPT1* and *TTP1*) also showed normal results.

The last physical examination at age 33 months revealed significant developmental delay: incapacity of sitting up unaided, failure to acquire language skills, and inability to smile. She still had seizures despite the ketogenic diet and the multiple seizure medications administered. A lack of visual pursuit associated with a vertical nystagmus was noted. Despite tube feeding, her height remained at the 14th centile, and her weight at the 3rd centile. She had microcephaly (OFC at the 4th centile) but no dysmorphic features. Despite intensive care, her medical condition deteriorated and she died at age 34 months.

Case 4 (Individual II-1, family C)

Individual 4 is a girl, the first-born child of non-consanguineous German parents. She was borm by caesarean section at 38 weeks of gestation after a normal pregnancy. The growth characteristics at birth were: weight 3.2 kg (M), length 53 cm (M) and OFC 34.5 cm (M). She

presented with congenital strabismus, which improved spontaneously at age 2 years. The electroretinogram was normal. She underwent bilateral hip dislocation surgery at age 11 months. At age 2 years and 6 months, she started having hypnagogic leg jerks. At age 4 years, another kind of abnormal movement appeared, consisting of involuntary head deviation with arm and leg extension. These movements, lasting less than 10 seconds, occurred only during sleep with a frequency of two or three times a night. They were absent when the child was awake and were efficiently controlled with clobazam. Waking EEG monitoring results were normal but spikes and sharp waves were present on awakening. Brain MRI, performed at age 3 years, showed a mild cerebellar hypoplasia without brainstem anomalies, white matter hyperintensities periventricular region (Figure 1B, d,i). Physical examination at age 6 years showed significant developmental delay: incapacity to sit up without help, and failure to acquire language skills. Axial hypotonia was associated with peripheral hypertonia. She also had severe growth retardation: length 98cm (-4SD), weight 12kgs (-5 D) and microcephaly OFC: 47.5cm (-2.5SD), despite adequate caloric intake. She had no dysmorphic features.

Case 5 (Individual II-2, family D)

Individual 5 is a girl, the fifth child born to non-consanguineous parents originating from Kuwait. She was born at 32 weeks of gestation after a normal pregnancy. Her birth weight was 2.6 kg. She had congenital stridor and required treatment for hyperbilirubinemia. Developmental delay became obvious from the age of 6 months. She was able to maintain mutual gaze but has never been able to sit up unaided or to develop language skills. At age 2 years, her neurological condition suddenly worsened during an acute infectious disease that required intubation and ventilation. At that time, she developed a severe dystonia, which did not improve with baclofen, clonazepam, L-DOPA and valproic acid. Dystonic movements gradually disappeared but, at age 5 years, another acute neurological deterioration occurred,

including spastic/dystonic movements, stridor, and dysphagia. Neurological examination at age 6 years was significant for severe spasticity with dystonia, repetitive and prolonged episodes of opisthotonus, dysphagia and poor visual pursuit. The EEGs were difficult to interpret because of continuous muscle artifacts even when using sedative drugs. However, severe slowing down of the background activity was observed, with some epileptiform discharges over the central and frontal areas. Nevertheless, the movement disorders such as opisthotonus and limb spasms were not caused by epileptic seizures.

In addition, she was microcephalic (OFC -2.4 SD) and showed signs of failure to thrive (length -4.7 SD, weight -4.8 SD) despite adequate caloric intake by enteral tube feeding. At that time, a percutaneous endoscopic gastrostomy was placed because of swallowing difficulties and poor nutritional status. Normal testing included plasma lactate, urine lactate/creatinine ration, urine amino and organic acids, plasma amino acids, plasma biotinidase activity, CDG screening, lysosomal disorder screening, karyotype, and a search for mutations in *SLC19A3*, the gene encoding for the thiamine transporter. Fortuitously, plasma levels of thyroid hormones were increased in the blood because of the existence of familial dysalbuminemic hyperthyroxinemia.

Brain MRI performed at age 9 months showed mild brain atrophy with normal myelination. Subsequent brain MRI at age 5 years showed a severe cortical atrophy with a thin corpus callosum and a cerebellar atrophy without brainstem anomalies (Figure 1B, e,j).

Figure S1. Sequence Alignment of *UBA5*

p.Met57Val

```
HUMAN         RIEKMSSEVVDSNPYSRLMALKRMGIVSDYEKIRTFA
ORANGUTANG    RIEKMSSEVVDSNPYSRLMALKRMGIVSDYEKIRTFA
MOUSE         RIQEMSDEVLDSNPYSRLMALKRMGIVSDYKKIRTYA
CHICKEN       RIETMSPEVTDSNPYSRLMALKRMGIVKDYEKIRTFT
ZEBRAFISH     KIEQMSAEVVDSNPYSRLMALKRMGIVQDYEKIRSFA
C-ELEGANS     KIEKLSAEVVDSNPYSRLMALQRMGIVNEYERIREKT
```

p.Gly168Glu

```
HUMAN         NITTVENFQHFMDRIS-NGGLEEGKPVDLVLSCVDNF
ORANGUTANG    NITTVENFQHFMDRIS-NGGLEEGKPVDLVLSCVDNF
MOUSE         NITTVEHFEHFMNRIS-NGGLEEGQPVDLVLSCVDNF
CHICKEN       NITTLDNFEHFMDRIS-NGALEEGKPVDLVLSCVDNF
ZEBRAFISH     NITTMDNFTHFMDRVRYHGGLEEGKPVDLILSCVDNF
C-ELEGANS     NITTMDNFDTFVNRIR-KGSLTDG-KIDLVLSCVDNF
```

p.Val260Met

```
HUMAN          KTLKREGVCAASLPTTMGVVAGILVQNVLKFLLNFGT
ORANGUTANG     KSLKREGVCAASLPTTMGVVAGILVQNVLKFLLNFGT
MOUSE          KTLKREGVCAASLPTTMGVVAGILVQNVLKFLLKFGT
CHICKEN        KTLKREGVCAASLPTTMGVVAGILVQNVLYFLLNFGT
ZEBRAFISH      KTLKRDGVCAASLPTTMGVVAGLLVQNVLYFLLGFGT
C-ELEGANS      RTLKRDGVCAASLPTTMAVVAGFLVMNVLYFLLNFGE
```

p.Ala371Thr

```
HUMAN         ELKNFSGPVPDLPEGITVAYTIPKKQEDSVTELTVED
ORANGUTANG    ELKNSSGPVPDLPEGITVAYTIPKKQEDSVTEVTVED
MOUSE         ELKNSSGPVPTLPEGITVAYTVPKKTEDSASEVTVED
CHICKEN       ELKAASGPVPDLPVGITVAYTIPNKEENLTAEETVAE
ZEBRAFISH     ELQDASGPIPDLPEGITVAYTIPEKDGGS--GETVEE
C-ELEGANS     AEQSSS---LNAGTGLKFAYEPIKRDAQT--EL--SP
```

p.Asp389Tyr

```
HUMAN         ITVAYTIPKKQEDSVTELTVEDSGESLEDLMAKMKNM
ORANGUTANG    ITVAYTIPKKQEDSVTEVTVEDSGESLEDLMAKMKNM
MOUSE         ITVAYTVPKKTEDSASEVTVEDSGESLEDLMARMKNM
CHICKEN       ITVAYTIPNKEENLTAEETVAESEESLEDLMAKMRNL
ZEBRAFISH     ITVAYTIPEKDGGS--GETVEETEQSLEELMAQMKKM
C-ELEGANS     LKFAYEPIKRDAQT--EL--SPAQAATHDFMKSIKDK
```

Figure S2: Biochemical Characterization of the Disease-Causing Mutations in UBA5 Protein using the Thioester Assay

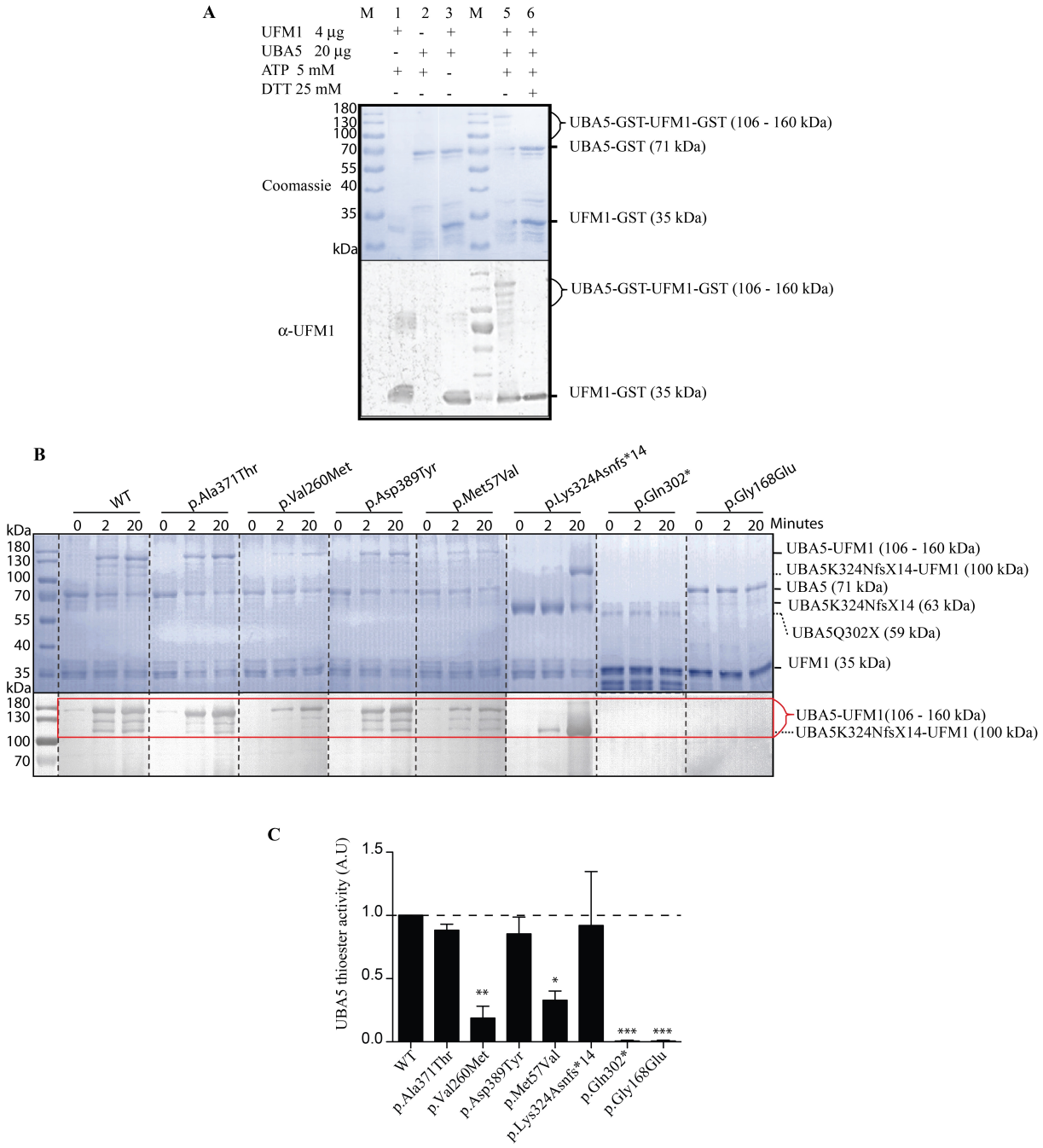

(A) **The thioester formation assay** was performed as described[1]. In the presence of ATP three bands containing UFM1-GST / UBA5-GST conjugates (range 106-160 kDa) were visible. They were excised and verified using MALDI/TOF mass spectrometry. The addition of DTT in the sample buffer led to the disappearance of these bands, confirming a thioester bond between the proteins. (B) **Time-dependent UFM1 activation assay.** UBA5-GST fusion proteins, each carrying one of the mutations of the affected families, were analyzed in a time-

dependent (0, 2 and 20 min) *in vitro* thioester formation assay. Sample reactions were subjected to SDS-PAGE and analyzed by coomassie staining (top) and immunoblotting using anti-UFM1 (1:2000) (bottom). Singular UFM1-GST and UBA5-GST proteins and the formed intermediates are indicated on the right. Three bands appeared (range 106-130 kDa) as a result of the thioester formation, representing UBA5-UFM1 intermediates highlighted by the red box. While the assay with wildtype (WT) UBA5 protein resulted in one band during the first seconds (130 kDa, time 0) and three strong bands (range 106-130 kDa) after 2 minutes (no increase after 20 min), the p.Val260Met and the p.Met57Val proteins displayed a highly significant reduction of UFM1-UBA5 conjugates ($p<0.001$) after 2 and 20 min. The p.Ala371Thr and the p.Asp389Tyr protein did not display significant differences in the UFM1 activation compared to the wildtype protein. The frameshift mutation p.Lys324Asnfs*14 showed a delayed activity ($p<0.001$, t-test), but was comparable to the wildtype after 20 min. The p.Gln302* and p.Gly168Glu proteins had no detectable thioester activity. (C) The thioester formation are observed after 20 minutes of incubation. Three independent experiments were used for quantification and statistical analyzes using One way ANOVA, Bonferroni's Multiple Comparaison test, * $p<0,05$, ** $p<0,01$, *** $p<0,001$.

Figure S3: Biochemical Characterization of the Disease-Causing Mutations in UBA5 Protein using the Trans-Thioester Assay

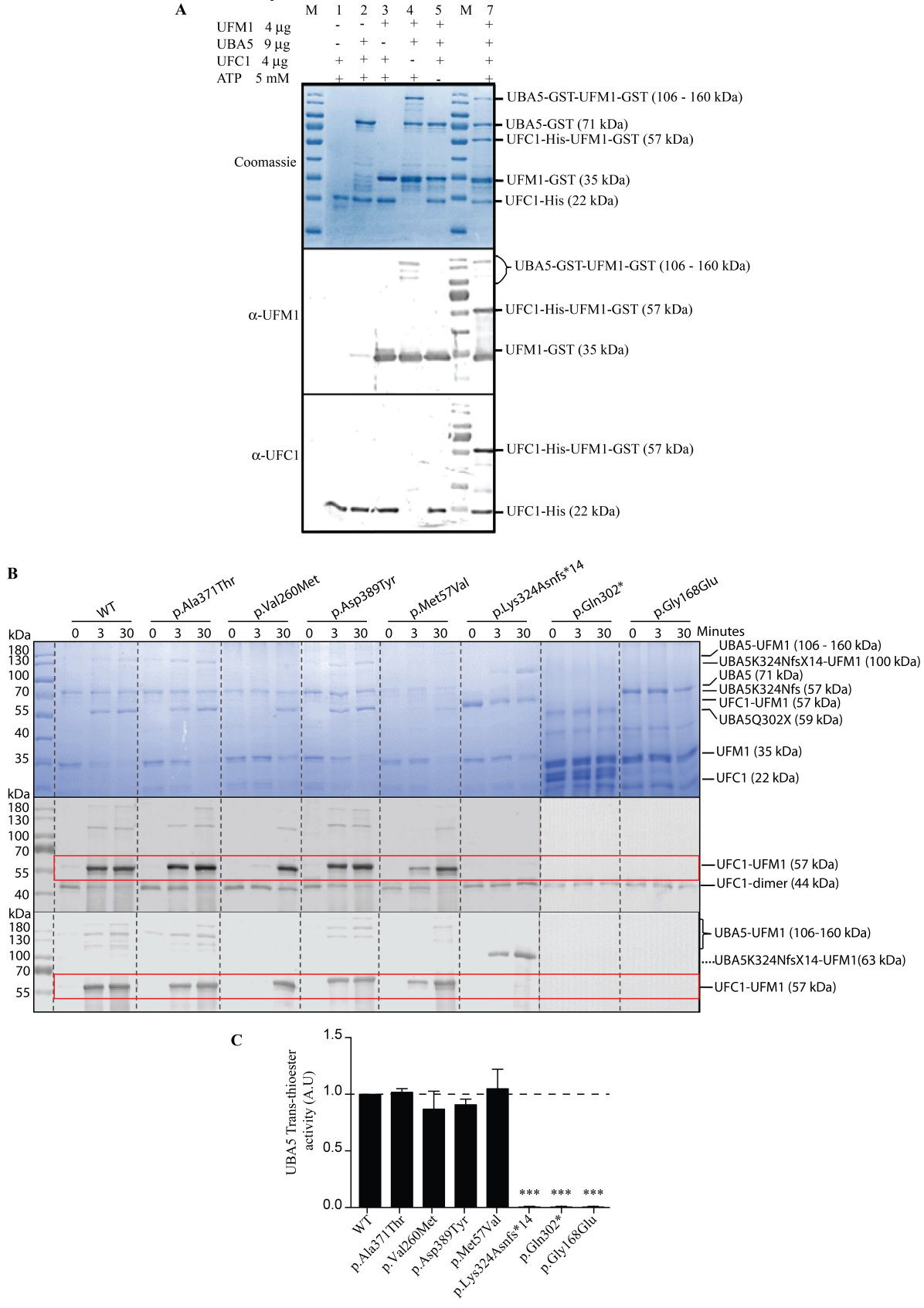

(A) The trans-thioester assay was performed as described[1]. In the presence of ATP, UFM1, UBA5 and UFC1, a band at 57 kDa containing UFM1-GST and UBA5-GST was observed additionally to the UFM1-GST / UBA5-GST conjugates at 106-160 kDA, therefore demonstrating trans-thioester activity of UBA5. (B) **Time-dependent UFM1 conjugation assay.** The UBA5-GST fusion proteins were analyzed in a time-dependent (0, 3 and 30 min) *in vitro* trans-thioester formation assay with UFC1. Sample reactions were subjected to SDS-PAGE and analyzed by coomassie staining (top) and immunoblotting using anti-UFM1 (1:2000) (middle), anti-UFC1 (1:10000) (bottom). Bands corresponding to singular UFM-GST, UBA5-GST and UFC-His as well as the intermediates are indicated on the right. Wildtype UBA5 was able to conjugate UFM1 to UFC1 within the first three minutes and the amount of conjugates did not increase significantly after 30 min. The p.Asp389Tyr, the p.Val260Met and the p.Met57Val proteins displayed a significantly reduced density of UFM1/UFC1 conjugate bands after 3 min ($p<0.05$), while no differences could be observed after 30 min. The conjugation activity of p.Asp389Tyr was not discernable from the wildtype protein. No conjugation activity was observed for the p.Gln302*, p.Gly168Glu and the p.Lys324Asnfs*14 proteins. (C) The trans-thioester formation are observed after 30 minutes of incubation. Three independent experiments were used for quantification and statistical analyzes using One way ANOVA, Bonferroni's Multiple Comparaison test, * $p<0,05$, ** $p<0,01$, *** $p<0,001$.

Figure S4: UBA5 Mutant Fibroblasts Are Resistant to Tunicamycin

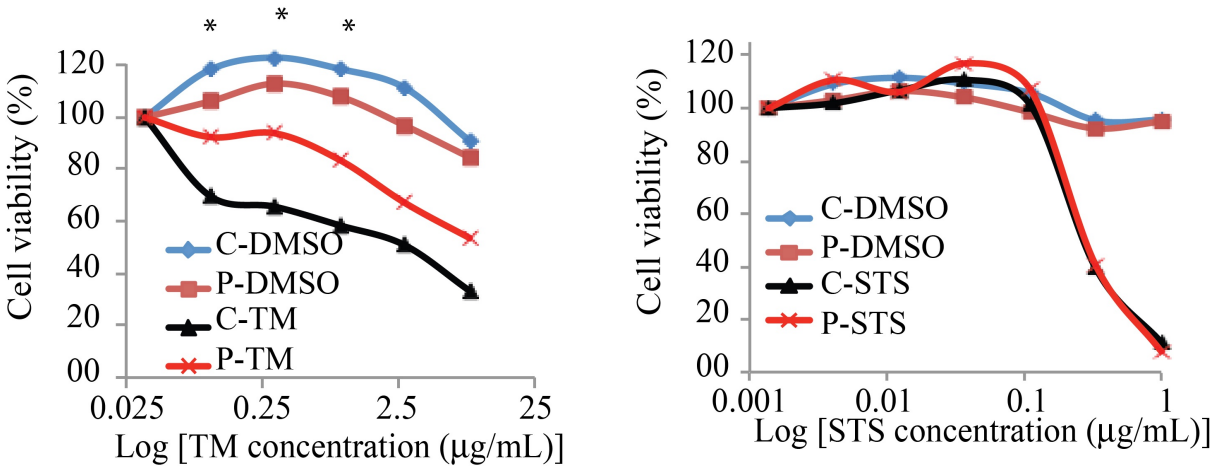

Cell viability assay after treatment with tunicamycin (TM, left) and staurosporine (STS, rigth). At day 3, cell viability was determined using Prestoblue Cell Viability reagent. DMSO was used as control in both TM and STS treatment. Abbreviations are as follow: C, wild type fibroblasts; P, *UBA5* mutant fibroblasts. Statistical analyzes: student t-test, $p<0.05$.

Figure S5: Neurological Characterization of *C. elegans* Strains Deleted for Genes Involved in Ufmylation

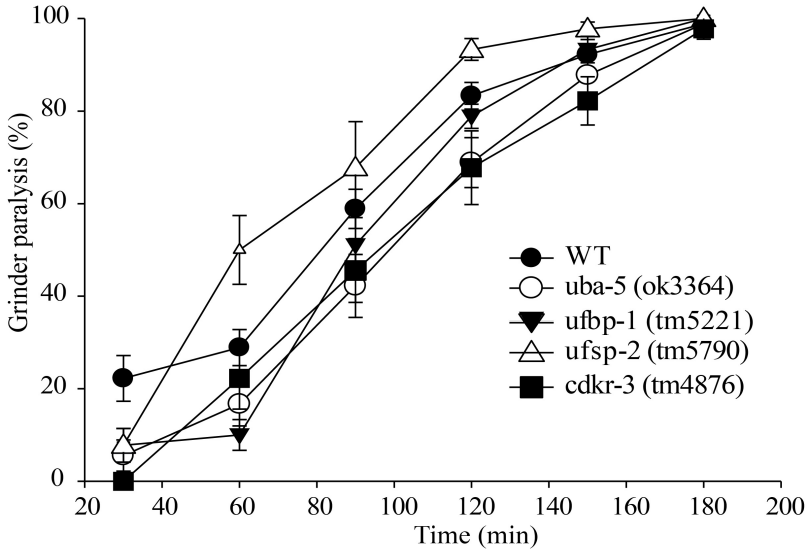

Levamisole exposure motility assay (0.4 mM levamisole, 3 h) revealed no significant difference using ANOVA test in the forward movement ability between the UFM-1 cascade deletion mutants and the WT.